Contents lists available at ScienceDirect

Tribology International

Spatiotemporal mapping for in-situ and real-time tribological analysis in polymer-metal contacts

Kian Kun Yap [a,b,*], Kanao Fukuda [b], Jennifer Renee Vail [c], Janet Wong [a], Marc Arthur Masen [a]

[a] *Tribology Group, Department of Mechanical Engineering, Imperial College London, United Kingdom*
[b] *Malaysia-Japan International Institute of Technology, Universiti Teknologi Malaysia, Malaysia*
[c] *Precision Parts and Solutions, Electronics and Industrial, DuPont de Nemours Inc, United States*

ARTICLE INFO

Keywords:
Polymers
Spatiotemporal mapping (SMA)
Transfer films
Triboscopy

ABSTRACT

Spatiotemporal mapping (SMA) is a graphical technique to visualise the evolution of data with time and space during a process. This paper discusses the benefits of SMA in the field of polymer tribology via two highly different polymer/metal sliding systems. The SMA is found useful for the qualitative and quantitative characterisation and analysis of the transfer phenomena at the contact interface during repeated sliding, e.g., the slide-roll mechanism of transfer lumps, the severe-to-mild wear transition due to the tribo-chemical reaction of PTFE, the accumulation of wear debris, and the formation of friction-reducing back-transfer polyimide films. Additionally, the SMA helps spot various abnormal tribological behaviours, such as the local removal of oxides on a misaligned disc that would otherwise be overlooked.

1. Introduction

Polymer/metal sliding interfaces are often employed in applications where liquid lubricants are unfavourable, e.g., at high temperatures, in vacuum, or when stringent contaminant tolerances apply. This is because they are less susceptible to seizure failure during dry sliding [1]. The coefficient of friction, μ of a polymer/metal sliding interface is typically low due to the transfer film formation mechanism [2]: during sliding, polymeric materials will exfoliate and adhere to the metallic surface to form a thin and uniform transfer film. This transfer film has a low shear strength, τ whilst the overall metallic substrate has a high hardness, H. According to the Bowden-Tabor adhesive friction model, this will result in low friction since friction is directly proportional to τ/H [3,4]. This transfer film formation mechanism contributes to the so-called self-lubrication of polymers. However, this 'textbook' explanation is an oversimplification of the actual conditions in a polymer/metal sliding interface, and ideal transfer films only form for a select group of linear thermoplastics, such as polytetrafluoroethylene (PTFE), high-density polyethylene (HDPE), and ultra-high-molecular-weight polyethylene (UHMWPE), and often this formation is limited to

specific operational conditions [2,5–7]. Most polymers, especially high-performance polymers (HPPs) tend to form more complex transfer films that are not uniform and continuously evolve [8–11]. The inclusion of blends and fillers in polymers further complicates transfer mechanisms [8,12]. Whilst such transfer films are generally believed to have an effect on the tribology of sliding systems, their exact functions remain unclear [8,13]. To better understand the tribological characteristics of transfer films, it is crucial to investigate the evolution of the transfer films during sliding, including their initiation, development, and removal [11,12]. However, the majority of research presented in literature focuses only on the post-hoc analysis of worn surfaces. In other words, the temporal information of local events during sliding is overlooked. An interesting possibility to overcome this is to apply the spatiotemporal mapping (SMA) technique to polymer tribology.

1.1. Basics of spatiotemporal mapping

In general, SMA is a three-dimensional visual representation of data in which the x-axis represents the spatial coordinate of the data, the y-axis represents the temporal coordinate, and the z-axis or the colour
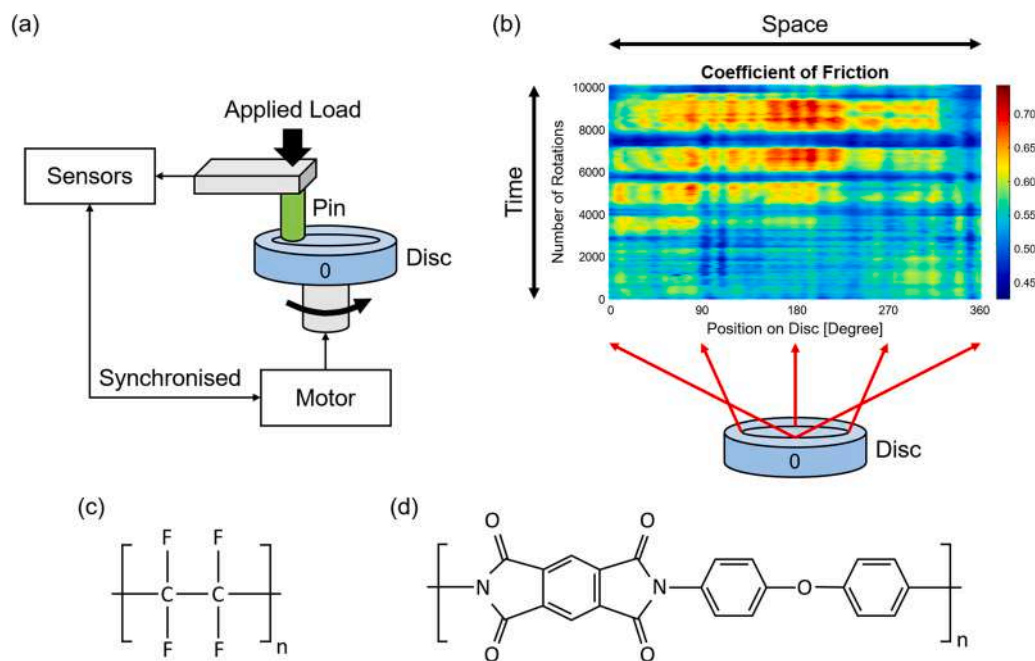

Fig. 1. (a) Schematic of a pin-on-disc setup, (b) example of an SMA of the coefficient of friction. The '0′ mark on the disc represents the starting point or the first point of contact in each repeated sliding cycle, and the chemical structures of (c) PTFE and (d) polyimide (PI).

intensity represents the numeric values of the data itself. This technique has been widely used in many fields, such as vibration monitoring [14, 15], medical diagnosis [16,17], geology [18,19], and weather forecasting [20,21]. In the field of tribology, SMA is often used in a pin-on-disc experiment, as shown in Fig. 1(a), and is sometimes referred to as triboscopy [22]. For a pin-on-disc experiment, the x-axis of an SMA may represent the position on the wear track of a disc, the y-axis represents the number of repeated sliding cycles, and the z-axis represents the magnitude of tribo-data, such as coefficient of friction, vertical pin position, or electrical contact resistance. An example of such an SMA is shown in Fig. 1(b) and typical SMA manifestations and their interpretations are presented in Supplementary Data. A vertical feature on an SMA suggests an event that occurs on the same position on the disc surface (Fig. S1); a horizontal feature means an event that happens on the pin surface (Fig. S2); whilst a diagonal feature implies an event that takes place on the disc but its position is changing during each repeated sliding cycle (Fig. S3). For a tribometer to generate a readable SMA, it requires a low noise, high sampling frequency, and high resolution data acquisition system that is synchronised by precise clock signals from a position transducer that is attached to the motion control system. The position transducer can be an encoder in a servo motor [23] or a position sensor such as a linear variable differential transformer (LVDT) [24]. The tribometer, ideally, should also have a function that allows the position of the first contact to be identified on the disc. This means any significant phenomena found on the SMA can be traced back to the corresponding position on the worn disc surface.

1.2. Spatiotemporal mapping in tribology

SMA was introduced into the field of tribology by Fukuda and Belin independently in 1992 [22,23]. The main focus of Fukuda et al. was the accumulation and the transfer of adhesive substances during the unidirectional repeated sliding of steels under dry [25–29] and boundary lubricated conditions [28,30]. In 2008, Fukuda proposed a new statistical analysis method based on the collected synchronised data to differentiate between abrasive and adhesive wear [31]. Belin et al. found that SMA is particularly useful for analysing the degradation and spalling of coatings during the reciprocating sliding of metals [32–36].

In 1994, Belin et al. implemented the SMA technique on an atomic force microscope (AFM) to characterise local wear evolution at the nanoscale [37]. Mello et al. recently improved Belin's technique and further extended the applications of SMA [24,38–41]. SMA has been successfully applied to analyse the in-situ and real-time dynamics of metal/-metal sliding contact but there is little literature available on the use of SMA for polymer/metal sliding interfaces. The only relevant work found was performed by Belin et al. in the early 1990 s on the sliding of polyvinyl chloride (PVC) coated aluminium against copper [22,32,33]. The current research aims to apply the SMA technique for elucidating the dynamic aspects of transfer films during polymer/metal sliding.

2. Material and Methods

Two highly different polymer/metal tribo-systems were investigated to explore the benefits of SMA, namely neat PTFE/AISI 304 ball-on-flat sliding at different humidity levels and graphite-filled sintered polyimide (PI)/AISI 52100 flat-on-flat sliding at elevated temperatures. PTFE is a thermoplastic addition polymer with a relatively simple structure, whilst PI is a pseudo-thermoplastic condensation polymer that has a more complex backbone. The tensile strengths of neat PTFE and PI are 15 MPa and 86 MPa respectively. Their chemical structures are shown in Fig. 1(c) and (d) respectively.
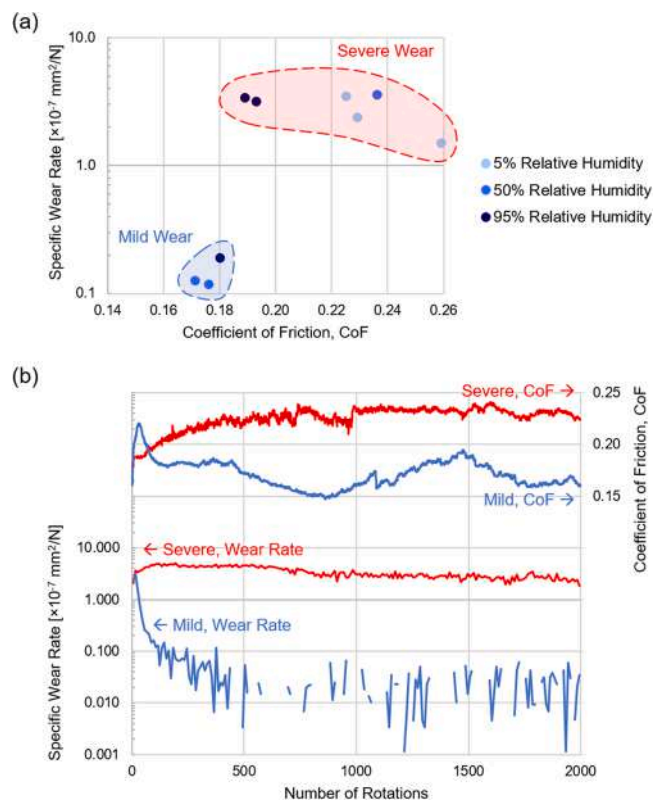
2.1. PTFE/AISI 304 sliding

The experiment was carried out utilising a custom-made pin-on-disc tribometer [42] and the contact mode was unidirectional ball-on-flat sliding. The stationary pins were made of 8 mm diameter neat PTFE balls and the rotating discs were made of 25 mm diameter AISI 304 stainless steel. The arithmetic surface roughness, Ra of the pins and discs were 0.52 μm and 0.02 μm respectively. Before the experiment, the PTFE pins were wiped with ethanol and the steel discs were ultrasonically cleaned with a 1:1 mixture of acetone and hexane for 10 min. After that, the discs were dried on a heat plate at 100 °C for 10 min to remove the solvents adsorbed on the surfaces. The discs were let to cool to room temperature before the sliding test commenced. The starting point of the motion was marked on the discs so that comparisons can be made

between the SMA and the worn disc surface after the sliding. The experiments were performed in a humidity-controlled chamber at 5%, 50%, and 95% relative humidity. The humidity was controlled by the mixing of dry and wet air, at an airflow rate of 10 litres per minute. Before each test, the PTFE specimens were kept in the humidity chamber for 30 min to make sure that the water adsorption on the surfaces had achieved a steady state [43]. All tests were performed at room temperature (24 °C). A 10 N dead weight was applied on the pin which is equivalent to a mean initial Hertzian contact pressure of 27 MPa. This contact pressure was calculated using the short-term Young's modulus of PTFE, which is 587 MPa [44]. Note that the Hertzian pressure exceeded the tensile strength of PTFE, meaning the contact is plastic. The initial contact diameter, 2a was 0.72 mm. This was obtained by pressing a PTFE ball against a transparent glass disc with a 10 N load and capturing contact using a microscope. The contact image is shown in Fig. S4. in Supplementary Data. The sliding speed was 60 rpm or 0.0628 m/s. The sampling rate was 720 Hz and the diameter of the wear track was 20 mm. This resulted in an SMA with a sampling interval of 87.3 μm. Each test lasted 2000 rotations or 125.7 m and at the end of the experiments, the diameter of the resulting wear scar of the pin ranged between approximately 1 mm and 2.6 mm. The friction force was measured by a strain-gauge-based load cell whilst the specific wear rate was calculated using the wear volume estimated by the diameter of the wear scar on the pin, and then divided by the normal load and the sliding distance. In addition, the vertical pin position was measured using an eddy current gap sensor. An increase in pin position means that the pin is raised, e.g., due to film build-up, whilst a decrease in pin position indicates wear of the surfaces. Each experiment was performed three times to check repeatability.

2.2. PI/AISI 52100 sliding

The experiment was conducted utilising a high temperature pin-on-disc tribometer (THT, Anton Paar, Austria) and the contact mode was unidirectional flat-on-flat sliding. The stationary pins were 4 mm diameter cylinders made of graphite-filled PI and the rotating discs were made of 50 mm diameter AISI 52100 bearing steel. PI specimens derived from pyromellitic dianhydride (PMDA) and oxydianiline (ODA) with 15 wt% and 40 wt% graphite fillers were tested in the experiment. Before the experiment, the PI pins were run-in using 2500 grit silicon carbide sandpaper which was attached to a disc on the tribometer for 1000 rotations to ensure good alignment and conformity between the contact surfaces. The pins were then wiped with isopropanol and new steel discs were ultrasonically cleaned with toluene for 15 min, followed by isopropanol for 5 min. The starting point of the motion was marked on the discs so that comparisons can be made between the SMA and the worn disc surface after the sliding. The arithmetic surface roughness, Ra of the pins and discs were 0.46 μm (after running in with sandpaper) and 0.12 μm respectively. The experiments were performed in a heat-controlled chamber at 100 °C, 300 °C, and 430 °C. During the experiments, the surrounding temperature was 20 °C and the humidity was ranging from 23% to 55%. The humidity variation is negligible for tests conducted at elevated temperatures. A 10 N dead weight was applied on the pin which is equivalent to a mean contact pressure of 0.8 MPa. The sliding speed was 120 rpm or 0.251 m/s. The sampling rate was 360 Hz and the diameter of the wear track was 40 mm. This resulted in an SMA with a sampling interval of 697 μm. Each test lasted 10,000 rotations or 1257 m. The friction force was measured using an LVDT-based flexural element whilst the specific wear rate was obtained using the wear volume calculated from the vertical pin position, which was measured using a rotary variable differential transformer (RVDT) sensor. The wear volume was divided by the normal load and the sliding distance to obtain the specific wear rate. An increase in pin position means that the pin is raised, e.g., due to film build-ups, whilst a decrease in pin position may indicate wear of the surfaces. Each test condition was performed three times to check the repeatability of the experiment.

Fig. 2. (a) Graph of average specific wear rate of the PTFE pin against average coefficient of friction for PTFE/AISI 304 sliding at different levels of relative humidity and (b) examples of the typical real-time specific wear rate and real-time coefficient of friction against number of rotations for severe (at 5% relative humidity) and mild (at 50% relative humidity) PTFE/AISI 304 sliding cases. Note that the discontinuity in the real-time specific wear rate for the mild wear case is due to the negative wear rate, implying the build-up of materials, which cannot be presented in a log scale graph.

3. Results and Discussion

3.1. PTFE/AISI 304 sliding

Fig. 2(a) shows the average specific wear rate of the PTFE pin and the average coefficient of friction for PTFE/AISI 304 sliding at different levels of humidity. It is difficult to study the effects of humidity on this tribology system as the results show poor repeatability, particularly for the average specific wear rate at 50% and 95% relative humidity, with values ranging from 0.12×10^{-7} to 3.59×10^{-7} mm²/N, which is a significant 30-time difference. The experiments that lead to a high wear rate or severe wear results are obtained on the specimens that exhibit high friction (data in the red region), whilst the low wear rate or mild wear results are characterised by low friction (data in the blue region). Fig. 2(b) shows the typical real-time specific wear rate and coefficient of friction for the full sliding cycles for severe and mild PTFE/AISI 304 sliding cases, which are taken from tests performed at 5% and 50% relative humidity respectively, to give a better picture of the friction and wear evolution during sliding. The real-time specific wear rate was calculated using the instantaneous wear volume, estimated by the change in vertical pin position every 10 rotations, and then divided by the normal load and the sliding distance in 10 rotations. Note that the discontinuity in the real-time specific wear rate for the mild wear case in Fig. 2(b) is due to the negative wear rate which cannot be presented in a log scale graph. A negative wear rate implies the build-up of materials in the contact which raises the pin during sliding.

It is found that all tests that lie in the same category, either severe wear or mild wear, have similar worn surface features, regardless of
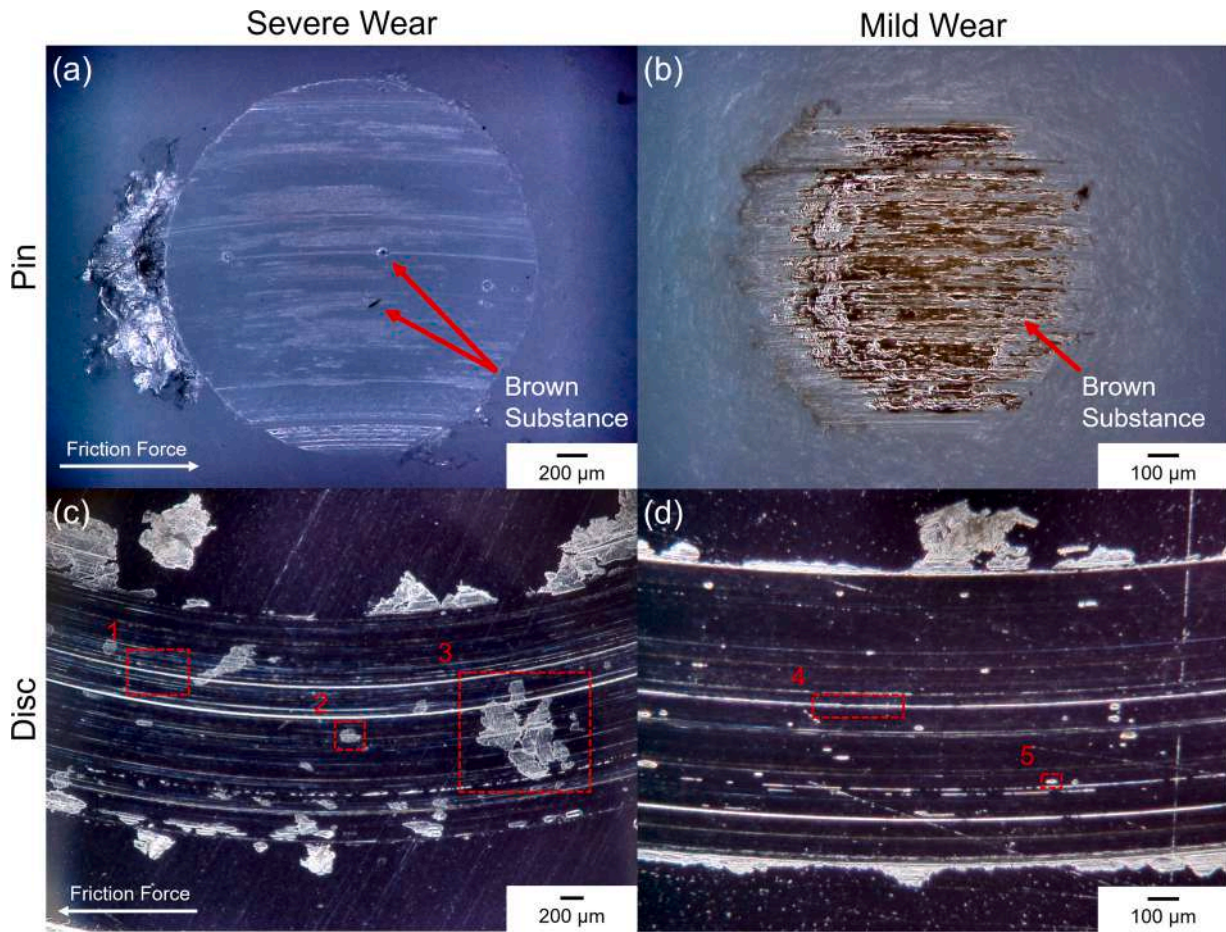
Fig. 3. Micrographs of (a, b) PTFE pins and (c, d) AISI 304 discs with severe and mild wear. The dotted red squares represent five typical types of PTFE transfer substances found on the disc wear tracks. Note that these micrographs were taken at different magnifications.

relative humidity. Therefore, hereafter, all results for severe and mild wear cases that are presented, are obtained from a 5% and a 50% relative humidity test respectively.

3.1.1. Micrographs of worn surfaces

To understand what causes the variation, the worn pin and disc surfaces for both severe and mild wear cases were observed under an optical microscope and the captured micrographs are presented in Fig. 3. Note that these micrographs were taken at different magnifications. The PTFE pin surface in the severe wear case (Fig. 3(a)) is much 'cleaner' compared to the mildly worn pin (Fig. 3(b)). There are not many foreign substances adhered to it. However, there is a large
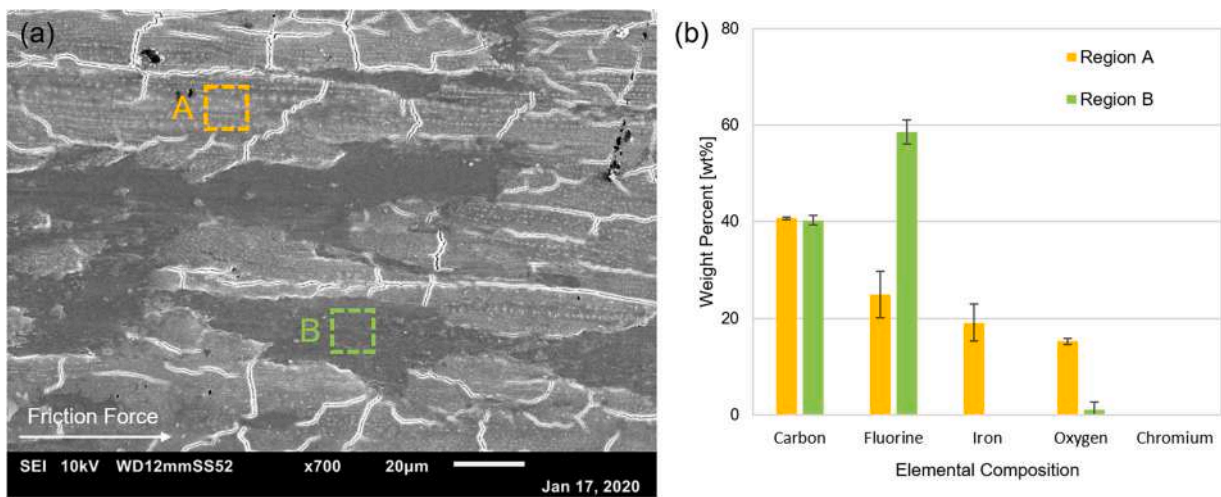
Fig. 4. (a) SEM image of a mildly worn PTFE pin surface and (b) the corresponding EDS analysis at region A and B. Region A is covered with a brown substance consisting of iron and oxygen elements, whilst region B is an uncovered PTFE surface. Each error bar in the graph represents the standard deviation that is obtained from measurements at three different locations on the worn pin surface.
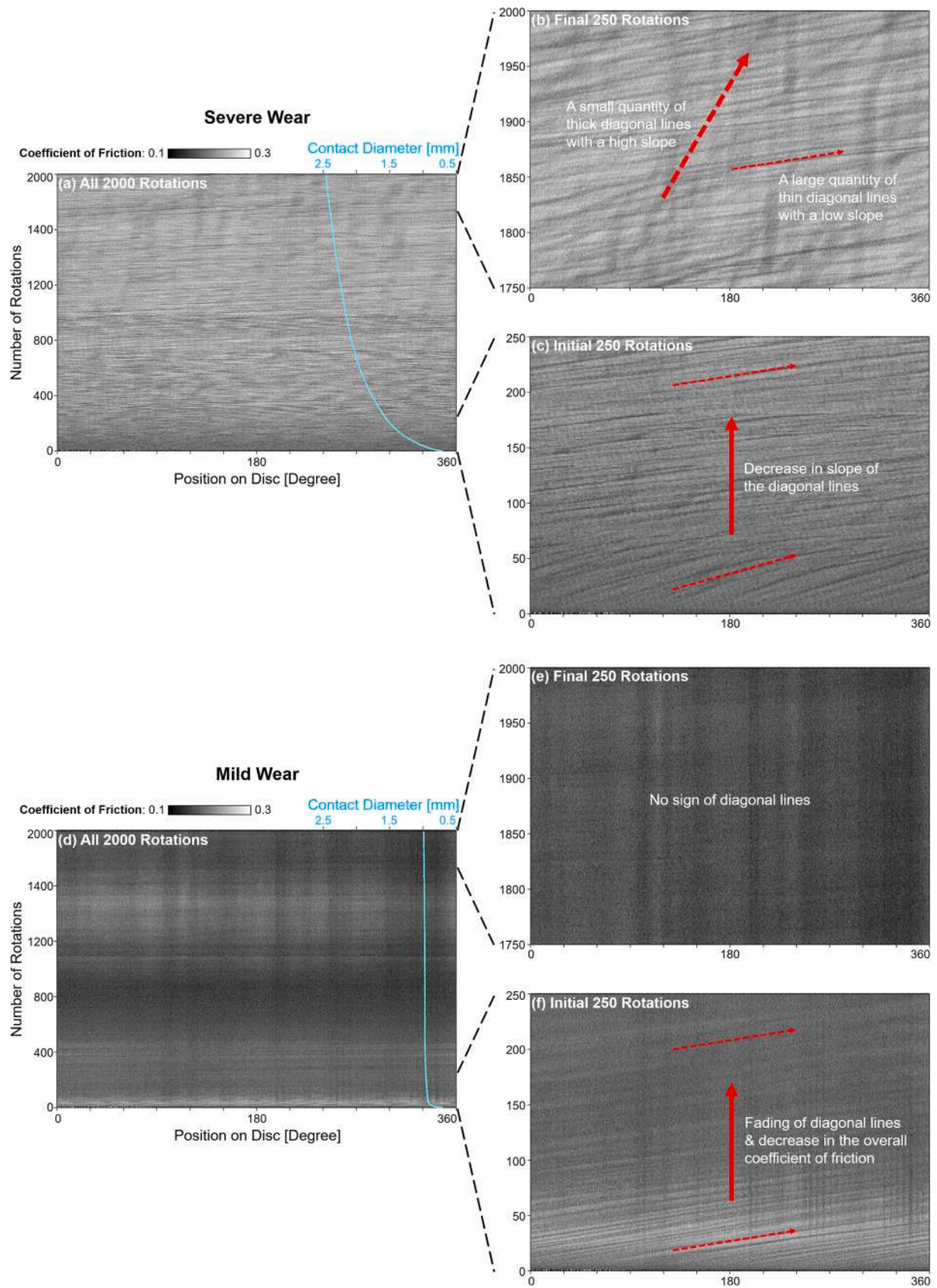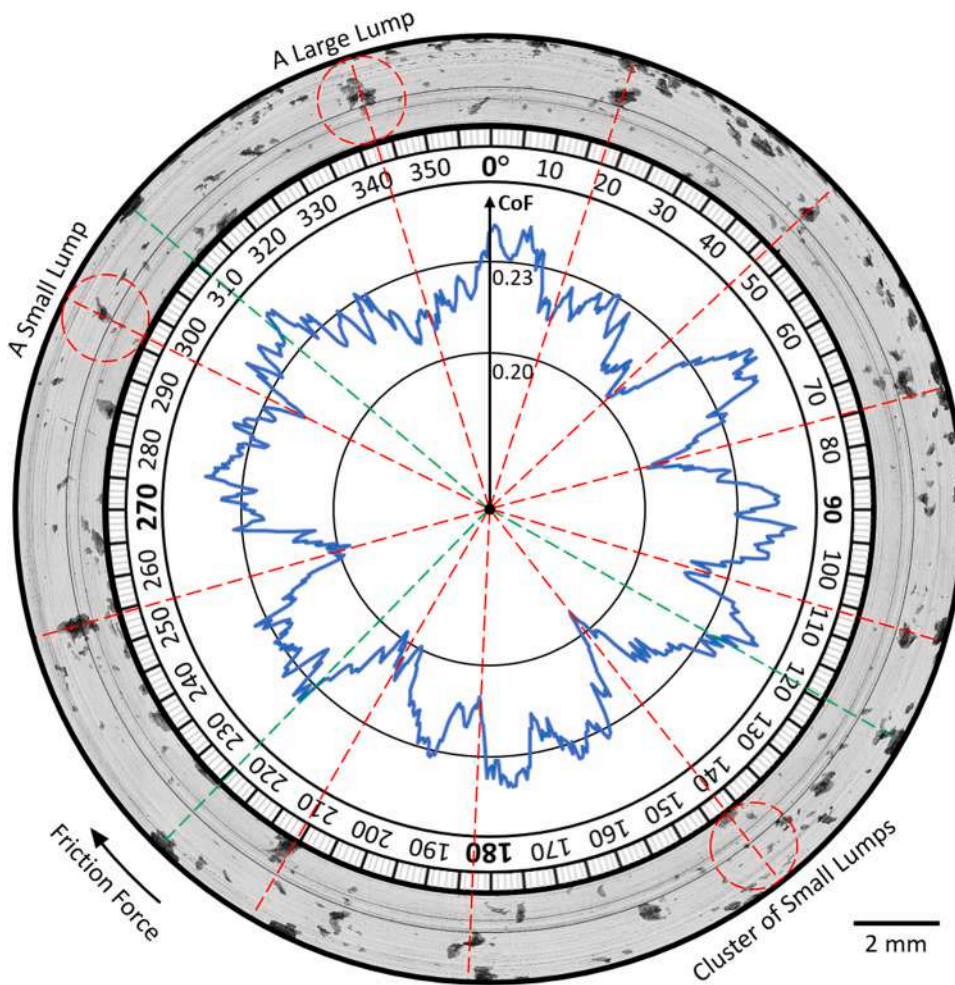
Fig. 5. SMAs of the coefficient of friction for (a – c) severe and (d – f) mild PTFE/AISI 304 sliding cases. The blue lines in (a) and (d) represent the calculated contact diameter against the number of rotations.

Fig. 6. Full rotation wear track of a severely worn disc and the corresponding coefficient of friction (CoF) for the last sliding cycle. The red dotted straight lines show that the positions where a significant reduction in CoF is found match well with the positions where significant PTFE transfer lumps are present at the centre of the wear track. The green dotted straight lines show that there is no significant decrease in CoF at positions where PTFE transfer lumps are present near the boundary of the wear track. The red dotted circles represent the size of a pin contact area.

quantity of adhered substances on the steel disc surface for the severe wear case (Fig. 3(c)), both in the wear track and outside of the wear track. These are PTFE materials that transfer from the pin to the disc and such transfer phenomena are commonly described in literature as a contributor to the self-lubrication of PTFE but the trade-off is the high wear rate [2]. The PTFE transfers manifest in various shapes and forms in this experiment. Based on the quantity, thickness, and width characterised by a laser scanning confocal microscope (refer to Fig. S5 in Supplementary Data), the authors categorise theseD transfer substances into three types as shown by the numbered labels in Fig. 3(c):

1. Thin transfer films: large total coverage, height < 0.1 µm, and oriented along the sliding direction;
2. Small transfer lumps: large quantity, height ≈ 1 µm, and diameter ≈ 200 µm; and
3. Large transfer lumps: small quantity, height > 1 µm, and diameter ≈ 600 µm.

For mild wear, the disc surface (Fig. 3(d)) is much 'cleaner' compared to the severely worn disc (Fig. 3(c)) with only a small number of PTFE transfers on it. These transfer substances can be categorised into two types as shown by the numbered labels in Fig. 3(d):

4. Thin transfer films: small total coverage, height < 0.1 µm, and oriented along the sliding direction; and
5. Tiny transfer lumps: large quantity, height between 0.1 µm and 1 µm, and diameter ≈ 30 µm.

The pin surface in the mild wear case (Fig. 3(b)) is covered with a dense brown substance. Fig. 4(a) and (b) show the scanning electron microscope (SEM) image and the energy-dispersive X-ray spectroscopy (EDS) analysis of the mildly worn PTFE pin surface respectively. The brown substance, as indicated by region A, consists of iron and oxygen elements. This suggests that they are materials that transfer from the steel disc to the pin. According to literature, the formation of this brown substance is attributed to the tribo-chemical reaction between steel and rubbed PTFE which becomes chemically active due to chain scission [45–49]. Wang et al. suggested that these substances are iron(III) oxides or Fe_2O_3 [50], whilst Campbell et al. proposed that they are chelated iron perfluorocarboxylates [49]. This iron-oxygen layer, which is marked as region A in Fig. 4(a), appears to be discontinuous and separated by cracks. The cracks are probably caused by the residual stress acting on the layer following stress relaxation of the PTFE substrate after sliding, which suggests a brittle nature of the layer. There are also patchy regions that are not covered with the iron-oxygen compounds, marked as region B. These uncovered regions may be caused by the delamination of the iron-oxygen layer from the PTFE surface. An AISI 304 stainless steel disc consists of 18 wt% chromium. The fact that no chromium is found on the pin surface as shown in Fig. 4(b) suggests that there is probably no tribo-chemical reaction between PTFE and chromium.

3.1.2. Spatiotemporal maps

Fig. 5(a) and (d) show the SMAs of the coefficient of friction for both severe and mild PTFE/AISI 304 sliding cases respectively, whilst Fig. 5 (b), (c), (e), and (f) are the zoomed-in SMAs for Fig. 5(a) and (d) at the initial and final stages of sliding. In these images, a brighter colour indicates a higher coefficient of friction. The evolution of the contact

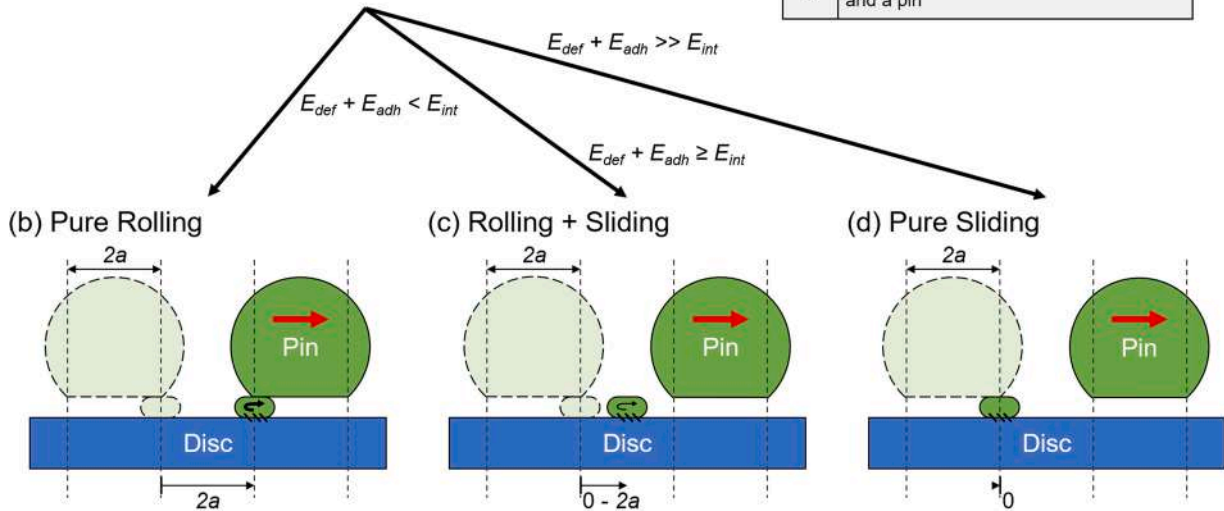## (a) Resistance Energy Experienced by a Transfer Lump
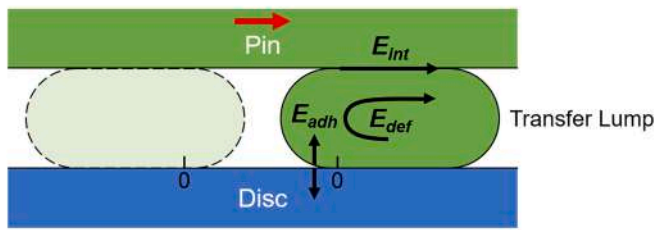
Annotation

E_{def}	Energy to plastically deform a transfer lump
E_{adh}	Energy to overcome the normal adhesion between a transfer lump and a disc
E_{int}	Energy to overcome the interfacial shear between a transfer lump and a pin
σ	Yield strength of a transfer lump
e	Average eccentricity of a transfer lump
s	Adhesion or sticking strength between a transfer lump and a disc
τ	Shear strength between a transfer lump and a pin

Rolling Resistance:

$$E_{def}(\sigma, e) + E_{adh}(s)$$

Sliding Resistance:

$$E_{int}(\tau)$$

$E_{def} + E_{adh} < E_{int}$

$E_{def} + E_{adh} \geq E_{int}$

$E_{def} + E_{adh} \gg E_{int}$

(b) Pure Rolling

2a

2a

(c) Rolling + Sliding

2a

0 - 2a

(d) Pure Sliding

2a

0

(e)

Coefficient of Friction: 0.1 ▬▬▬ 0.3

High Friction   Low Friction   High Friction

Number of Rotations vs Position on Disc [Degree]

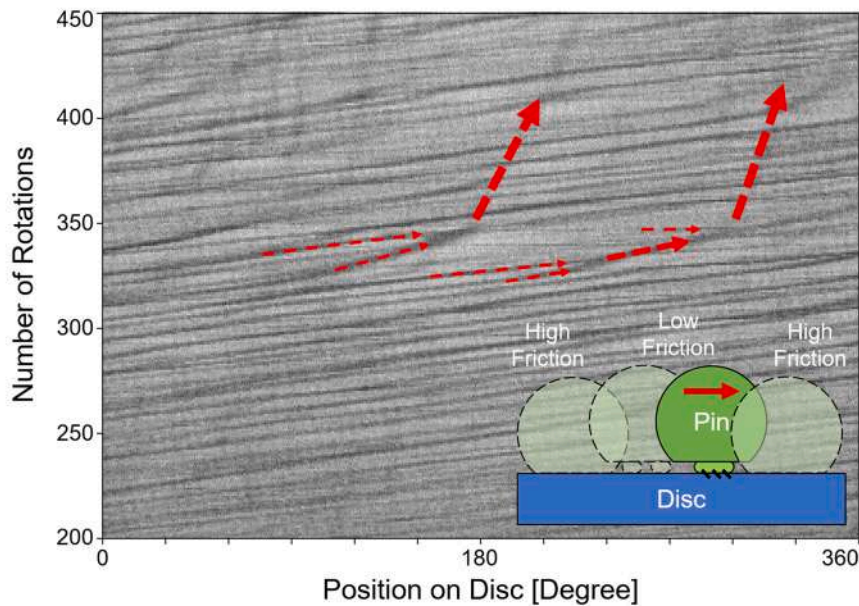**Fig. 7.** (a) Illustration of the proposed resistance energy experienced by a transfer lump during (b) pure rolling, (c) rolling and sliding, and (d) pure sliding. (e) illustrates the merging of small transfer lumps into a large transfer lump which is manifested on the SMA as the initiation of a thicker diagonal line with a higher slope at the intersection of two thinner diagonal lines with lower slopes.

diameter due to wear during both severe and mild wear cases are presented as the blue lines in Fig. 5(a) and (d). The initial contact diameter is 0.72 mm for both cases. The contact diameter during sliding was calculated using the measured real-time vertical pin position and the geometry of a spherical cap. For severe wear, the calculated contact diameter at the last rotation is 2.46 mm, whilst the measured diameter of the pin wear scar is 2.43 mm. For mild wear, the calculated contact diameter at the last rotation is 0.99 mm, whilst the measured diameter of the pin wear scar is 1.07 mm. There is high agreement between the calculated contact diameter at the last rotation and the measured diameter of the pin wear scar for both cases suggests that the calculated real-time contact diameters are accurate.

In general, the SMA for severe wear (Fig. 5(a)) shows higher friction than mild wear (Fig. 5(d)) and a complex pattern with rapid friction fluctuations can be observed. Zooming in to the initial 250 rotations (Fig. 5(c)), these friction fluctuations reveal as diagonal lines with lower friction and the slope of these lines decreases with time. In the final 250 rotations (Fig. 5(b)), these diagonal lines continue, and additionally, a new diagonal line variant is found. These lines are thicker, have a higher slope, and are present in a smaller quantity. For mild wear (Fig. 5(d)), the friction is lower compared to severe wear and alternating horizontal intervals of reduced and elevated friction are observed. Zooming in to the initial 250 rotations (Fig. 5(f)), diagonal lines with lower friction are also found but these lines fade with time. In the final 250 rotations (Fig. 5(e)), these diagonal lines have disappeared.

3.1.3. Severe wear

The 'clean' severely worn PTFE pin surface, which does not have significant traces of iron-oxygen compounds, (Fig. 3(a)) in combination with a disc covered with PTFE substances (Fig. 3(c)) indicates the transfer of materials from the pin to the disc during severe wear. It is inferred that these PTFE transfer substances cause the diagonal lines with reduced friction on the SMA as shown in Fig. 5(a – c). Fig. 6 shows the full rotation wear track of a severely worn disc and the corresponding coefficient of friction for the last sliding cycle. The positions where a significant reduction in friction is found match well with the positions where significant PTFE transfer lumps are present as shown by the red dotted straight lines. These transfer lumps are mainly located at the centre of the wear track. There is no significant decrease in friction at positions where transfer lumps are located closer to the boundary of the wear track as shown by the green dotted straight lines. This confirms that the diagonal lines with low friction are formed when the pin slides across the PTFE transfer lumps that are located at the centre of the wear track. When this occurs, the contact interaction is mainly between PTFE and PTFE, resulting in reduced friction. The fact that these lines are diagonal suggests that the transfer lumps are moved gradually by the pin along the wear track of the disc in each repeated sliding cycle (refer to Fig. S3 in Supplementary Data). This phenomenon of the gradual displacement of transfer lumps was also reported by Ye et al. during the sliding of PTFE against smooth stainless steel surfaces [51].

The SMA suggests the gradual displacement of the transfer lumps on the disc but the displacement mechanism, e.g., whether the transfer lumps slide or roll on the surfaces, remains unclear. Fig. 7(a) hypothesises the resistance energy experienced by a transfer lump at the contact interface during sliding. In order for the transfer lump to roll, it would need to overcome both the deformation energy, E_{def} and the adhesion energy, E_{adh}. E_{def} is the energy required to plastically deform the transfer lump, which is a function of the yield strength, σ and the average eccentricity, e of the transfer lump, whilst E_{adh} is the energy required to overcome the adhesion between the transfer lump and the disc, which is a function of the adhesion or sticking strength, s between the two surfaces. The average eccentricity, e is defined as how much a body deviates from a perfect round, which adds rolling resistance to the body to overcome plastic deformation. In order for the transfer lump to slide, it would need to overcome the interfacial energy, E_{int}, which is the energy required to overcome the interfacial shear between the transfer lump and the pin, which is a function of the shear strength, τ

between the two surfaces.

If the rolling resistance ($E_{def} + E_{adh}$) is smaller than the sliding resistance (E_{int}), the transfer lump would experience pure rolling (Fig. 7(b)) and the displacement of the lump on the disc should be equal to the contact diameter, $2a$. If the rolling resistance is much greater than the sliding resistance, the transfer lump would experience pure sliding (Fig. 7(d)) and there should be zero displacement between the lump and the disc. If the rolling resistance is equal to or slightly greater than the sliding resistance, the transfer lump would experience both rolling and sliding (Fig. 7(c)) and its travel distance on the disc should be between zero and $2a$. The distance travelled by a transfer lump on the disc during sliding can be quantified using the slope of the diagonal lines on an SMA. This slope represents the number of rotations required by the pin to move a transfer lump on the disc by one degree. In other words, the higher the slope of a diagonal line, the shorter the distance the transfer lump is moved in one rotation, the lower the 'mobility' of the transfer lump, the more dominant the sliding mechanism over the rolling mechanism.

During the early stages of sliding (Fig. 5(c)), the slope of the diagonal lines is approximately 0.27 rotation/degree (or 0.65 mm/rotation) whilst the contact diameter, $2a$ is approximately 0.72 mm (Fig. 5(a)). The slope decreases with time to 0.16 rotation/degree (or 1.09 mm/rotation) at the 60th rotation. By this time, the contact diameter is approximately 1.10 mm. The fact that the distance travelled by the transfer lumps in one rotation is close to the contact diameter suggests that the transfer lumps experience mainly rolling during the first 60 rotations. The coefficient of friction is almost constant during the first 60 rotations as shown in Fig. 2(b). After the 60th rotation, it is interesting that the slope of the diagonal lines remains at a similar level (Fig. 5(c)) although the contact diameter keeps increasing (Fig. 5(a)). This indicates that the displacement mechanism begins to shift from rolling dominant to more sliding and the coefficient of friction starts to increase as shown in Fig. 2(b).

In the later stages of sliding (Fig. 5(b)), these diagonal lines on the SMA continue and their slope remains similar at 0.16 rotation/degree (or 1.09 mm/rotation). An additional diagonal line variant develops with a smaller quantity, a thicker line, and a higher slope, which ranges from approximately 0.71 rotation/degree (or 0.25 mm/rotation) to infinity rotation/degree (or 0 mm/rotation). Relating the positions of the two types of diagonal lines on the SMA (Fig. 5(b)) to the transfer lumps found on the disc wear track (Fig. 6), a thinner diagonal line with a lower slope corresponds to a smaller transfer lump (e.g., the lump at 297° in Fig. 6), whilst a thicker diagonal line with a higher slope correspond to a larger transfer lump (e.g., the lump at 343° in Fig. 6) or a cluster of small transfer lumps in the pin contact area (e.g., the lumps at 142° in Fig. 6). This indicates that the larger the transfer lumps or the larger the total transfer lump coverage in the contact area, the lower their mobility, and the more dominant the sliding mechanism over the rolling mechanism.

The fact that a larger transfer lump results in a higher slope on the SMA shows that the mobility of a transfer lump depends on its size. However, what causes the size variation in the transfer lumps remains unclear. It is found that the thick diagonal lines with high slopes, which represent large transfer lumps, are only present at the later stages of sliding (Fig. 5(b)), whilst the thin diagonal lines with low slopes, which represent small transfer lumps, can already be observed during the early stages of sliding (Fig. 5(c)). Based on this, it is hypothesised that most transfer lumps are initially small and may grow by merging with other small lumps during sliding. The initiation of a thicker diagonal line with a higher slope at the intersection of two thinner diagonal lines with lower slopes, as shown in Fig. 7(e) appears to support this hypothesis. Evidence that substantiates this hypothesis is the clear boundaries observed in the large transfer lump which is shown in label 3 in Fig. 3(c).

To sum up, severe wear is characterized by a large quantity of transfer from the pin to the disc in the form of lumps. These lumps are not stationary, but moved by the pin during repeated sliding, which manifests as diagonal lines with reduced friction on the SMA as shown in Fig. 5(a – c). The high mobility of the lumps enables some to be pushed out of the wear track as shown in Fig. 3(c). With time, transfer lumps
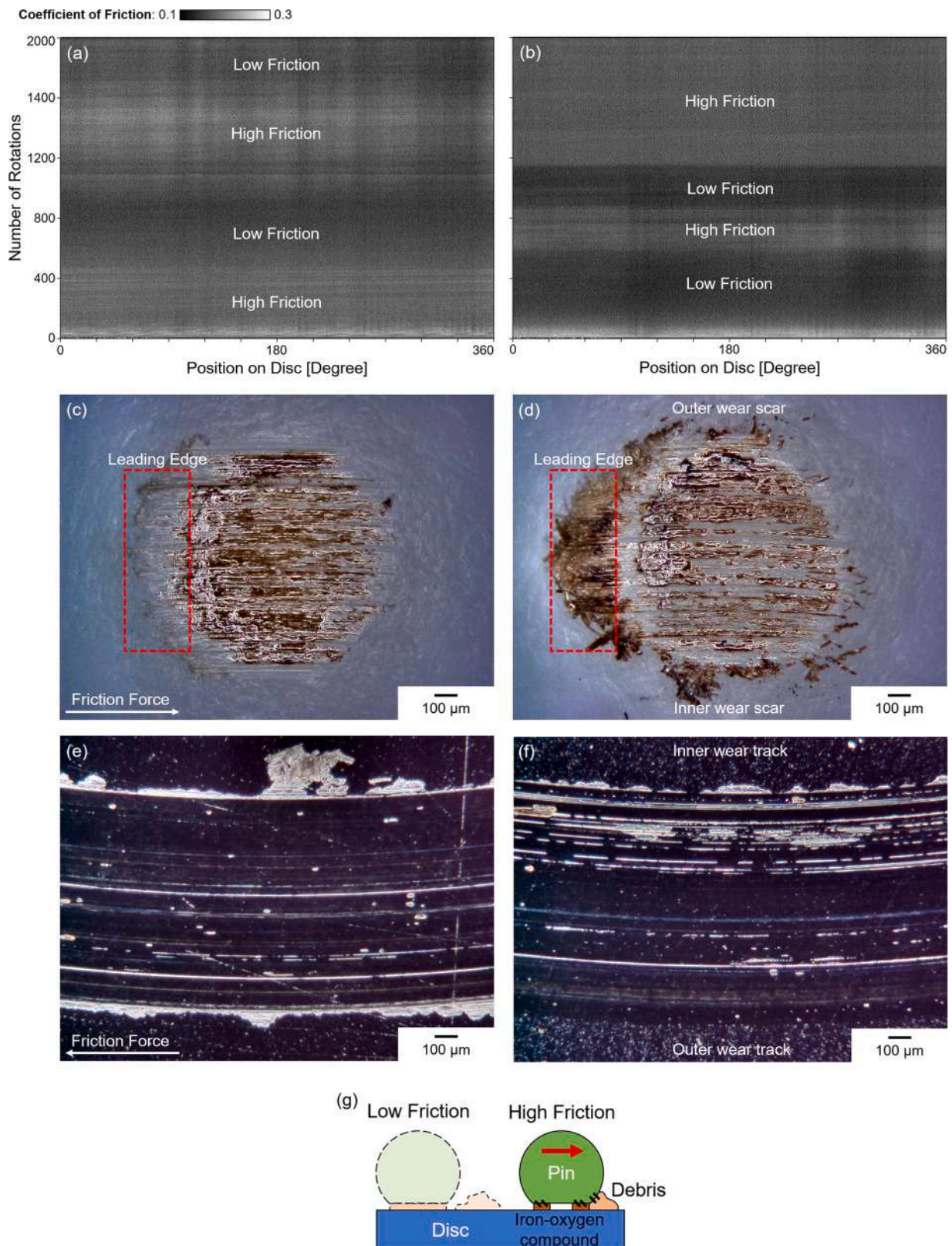
Fig. 8. Mild wear PTFE/AISI 304 sliding which ends in a low friction regime (a) has no noticeable accumulation of wear debris at the leading edge and has a more uniform iron-oxygen layer on the pin surface (c) and less PTFE transfer on the disc surface (e). The same sliding which ends in a high friction regime (b) has a large quantity of accumulated wear debris at the leading edge and has a less compact iron-oxygen layer at the inner wear scar on the pin surface (d) and more PTFE transfer at the inner wear track on the disc surface (f). (g) illustrates the process of the accumulation of wear debris and the partial removal of iron-oxygenlayers on the pin.

merge and form larger lumps that have lower mobility. Similar phenomena were reported by Ye et al. during the sliding of PTFE against smooth stainless steel surfaces [51]. It is hypothesised that if the sliding tests were to run for a longer duration, more of these larger lumps will form and eventually, a non-mobile and uniform protective film may form on the disc surface, lowering the overall friction and wear.

3.1.4. Mild wear

Mild wear (Fig. 5(d)) correlates to lower friction than severe wear (Fig. 5(a)). For mild wear, the pin is covered with iron-oxygen compounds (Fig. 3(b)), whilst the disc surface does not show significant traces of PTFE transfer (Fig. 3(d)). This indicates that the main contact interaction is iron-oxygen compound/steel. Similar to severe wear, the SMA shows diagonal lines with low friction during the early stages of sliding (Fig. 5(f)), implying the presence and gradual displacement of transfer lumps on the disc. This is accompanied by a high wear rate (10^{-7} mm^2/N), which is of the same order as the severe wear case, as shown in Fig. 2(b). This suggests that the sliding which results in overall mild wear commences as severe wear. These diagonal lines fade quickly with time and disappear in the later stages of sliding (Fig. 5(c)). This phenomenon is accompanied by a rapid drop of the real-time specific wear rate by two orders of magnitude to 10^{-9} mm^2/N, as shown in Fig. 2(b), indicating a transition to mild wear. The severe-to-mild wear transition is due to the transfer of iron from the disc to the pin which forms a protective layer (Fig. 3(b)) that prevents further transfer of PTFE from the pin to the disc. This is supported by the fact that the disc surface (Fig. 3(d)) does not show any clear traces of PTFE transfer. This implies that the formation of the iron-oxygen protective layer has to occur in the early stages of sliding as otherwise the disc will be covered with a large of quantity of transfer lumps already.

The slopes of the diagonal lines start at approximately 0.16 rotation/degree (or 1.09 mm/rotation) and remain similar during the early stages of sliding as shown in Fig. 5(f). Similar to the severe wear case, the distance travelled by the transfer lumps is limited to 1.09 mm/rotation. The reason for this is unclear but it is believed to be related to the balance between E_{adh}, E_{def}, and E_{int} of the system. The calculated contact diameter changes from 0.72 mm to 0.99 mm throughout the sliding as shown by the blue line in Fig. 5(d). This indicates that the distance travelled by the transfer lumps is always greater than the calculated contact diameter during the sliding. This suggests that the actual contact diameter may be larger than the calculated contact diameter during mild wear. This may be due to the accumulation of wear debris which is sometimes found at the leading edge of a mildly worn pin as shown in Fig. 8(d). Another hypothesis is that the transfer lumps have already been pushed ahead by the pin at the leading edge of the contact before they even enter the contact.

Zooming out to the SMA for the entire test as shown in Fig. 5(d), alternating horizontal intervals of reduced and elevated friction are observed. This horizontal feature indicates a change in tribological phenomena on the pin (refer to Fig. S2 in Supplementary Data). Fig. 8 shows the SMAs for mild wear, with Fig. 8(a) representing a test ended in a low friction regime whilst Fig. 8(b) representing a test ended in a high friction regime. The corresponding pin surface micrographs are shown in Fig. 8(c) and (d), whilst the disc surface micrographs are shown in Fig. 8(e) and (f) respectively. Experiments ending in a low friction regime have no noticeable accumulation of wear debris at the leading edge and have a uniform iron-oxygen layer on the pin surface (Fig. 8(c)), whilst experiments ending in a high friction regime show a large quantity of accumulated wear debris at the leading edge and a less uniform iron-oxygen layer on the pin surface (Fig. 8(d)). This suggests that the alternating horizontal intervals of low and high friction observed on the SMA are the result of:

1. The constant removal and build-up of wear debris at the leading edge of the pin contact; and/or
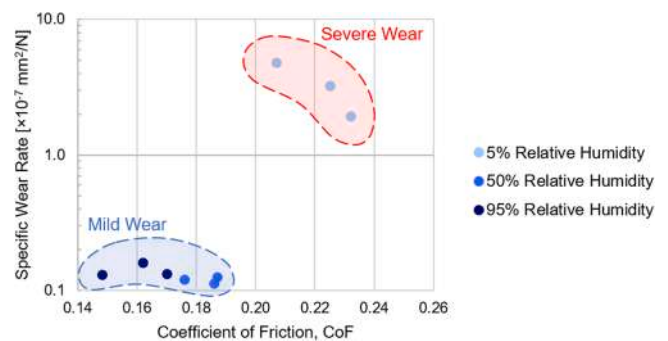2. The partial build-up and removal of iron-oxygen layers on the pin surface.

Fig. 9. Graph of average specific wear rate against coefficient of friction for PTFE/AISI 304 sliding at different levels of relative humidity when the discs had been heated for 60 min at 100 °C prior to the experiment.

This is illustrated in a schematic shown in Fig. 8(g). The increase in friction may be due to the accumulation of wear debris at the leading edge of the pin contact which increases the real contact area and subsequently the adhesive force. It may also be due to the partial removal of the iron-oxygen layer on the pin surface. The fact that a less compact iron-oxygen layer is found at the inner wear scar on the pin surface (Fig. 8(d)), whilst more PTFE transfer is found at the inner wear track on the disc surface (Fig. 8(f)) indicates local severe wear in the sliding contact which leads to higher friction.

3.1.5. Severe-to-mild wear transition

The discussion so far has only focused on what happens during severe and mild wear cases but it is still unclear what causes the poor repeatability of experiments performed at identical conditions as shown in Fig. 2(a). In Fig. 3(a), minor traces of iron-oxygen compound can be distinguished on the severely worn pin, possibly indicating that iron is transferred onto the pin surface but fail to develop into an effective protective layer. It is therefore important to investigate the mechanisms involved in the formation of a stable iron-oxygen layer, which is responsible for the severe-to-mild wear transition.

Two competing transfer mechanisms have been observed in these experiments, namely the transfer of PTFE from the pin to the disc, leading to severe wear and the transfer of iron from the disc to the pin, leading to mild wear. The diagonal lines in Fig. 5(c) and (f) indicate that the transfer of PTFE from the pin to the disc commences in the first 10 rotations. This means that to prevent severe wear, the iron-oxygen layer needs to develop on the pin surface within the first 10 rotations. These iron-oxygen compounds can be released from the existing oxide layer on the stainless steel surface, which consists of chromium oxide and iron oxide, or alternatively from a tribo-chemical reaction between the stainless steel and the PTFE [49,50].

The tribo-chemical reaction could be a continuous source of iron-oxygen compounds to maintain the protective layer on the pin. However, the transfer of PTFE to the stainless steel disc usually takes place prior to this tribo-chemical reaction [52,53]. It takes time for the shearing of PTFE to cause sufficient chain scission to enable the tribo-chemical reaction. Additionally, the existing chromium oxide layer on the stainless steel disc may need to be removed to expose iron for the tribo-chemical reaction. Therefore, it is hypothesised that the existing oxide layer on the stainless steel disc is important in delaying and reducing the transfer of PTFE to the stainless steel disc during the very early stages of sliding before tribo-chemical reaction takes place and initiates a continuous supply of iron-oxygen compounds. This also suggests that the poor repeatability of the experiments could be due to variations in the existing oxides that are present on the disc surface.

To verify this, a further experiment was conducted in which additional oxides were introduced to the disc surface by heating disc samples to 100 °C for 60 min prior to performing sliding tests. EDS analysis showed a 30% increase of oxygen on the surface as compared to the discs

used in the previous experiment. Fig. 9 shows the average specific wear rate plotted against the coefficient of friction at different levels of humidity. Much better consistency of friction and wear results was obtained. Mild wear is observed at 50% and 95% humidity, whilst severe wear is observed at 5% humidity. This experiment suggests that a larger amount of existing oxide on the disc helps maintain a stable iron-oxygen protective layer and promotes severe-to-mild wear transition for tests performed at 50% and 95% humidity. Additionally, it suggests that water, either as vapour in the air or as an adsorbed layer on the surface, is required for the formation and the maintaining of iron-oxygen protective layer on the pin. According to Campbell et al., water moisture in air is required for the carboxylation of PTFE before being able to form iron-chelates which make up the protective layers [49].

3.2. PI/AISI 52100 sliding

Fig. 10(a) and (b) show the coefficient of friction and the average specific wear rate for graphite-filled PI/AISI 52100 sliding at different surface temperatures. In general, the friction of the 40 wt% graphite-filled PI (green triangle markers) is lower than that of the 15 wt% graphite-filled PI (orange square markers). The higher graphite content reduces the overall shear strength of the polymer composite [54], resulting in lower friction according to the Bowden-Tabor model [3,4]. The toughness of the PI composite, defined as the product of tensile strength and elongation at break [54], also reduces which, according to the Ratner-Lancaster model, makes the material more prone to abrasion and brittle fracture, which should result in an increased wear rate [55,56]. However, the measured wear rate of the 40 wt% graphite-filled PI was no higher than that of the 15 wt% graphite-filled PI. This suggests that the main mechanism involved in the wear process is dominated by interfacial aspects such as adhesion, rather than bulk material aspects. The observed trends of friction and wear for both types of PI are similar. At 100 °C, friction is high whilst wear is low; at 300 °C, friction decreases sharply whilst wear increases slightly; and at 430 °C, friction is high again whilst wear increases sharply. In literature, these variations are mainly due to the change in the thermo-chemistry of the PI matrix that alters the mobility of the polymer chains. These processes, namely hydrolysis at 100 °C, imidisation at 300 °C, and oxidative degradation at 430 °C have been discussed extensively by other researchers [54,57–60].
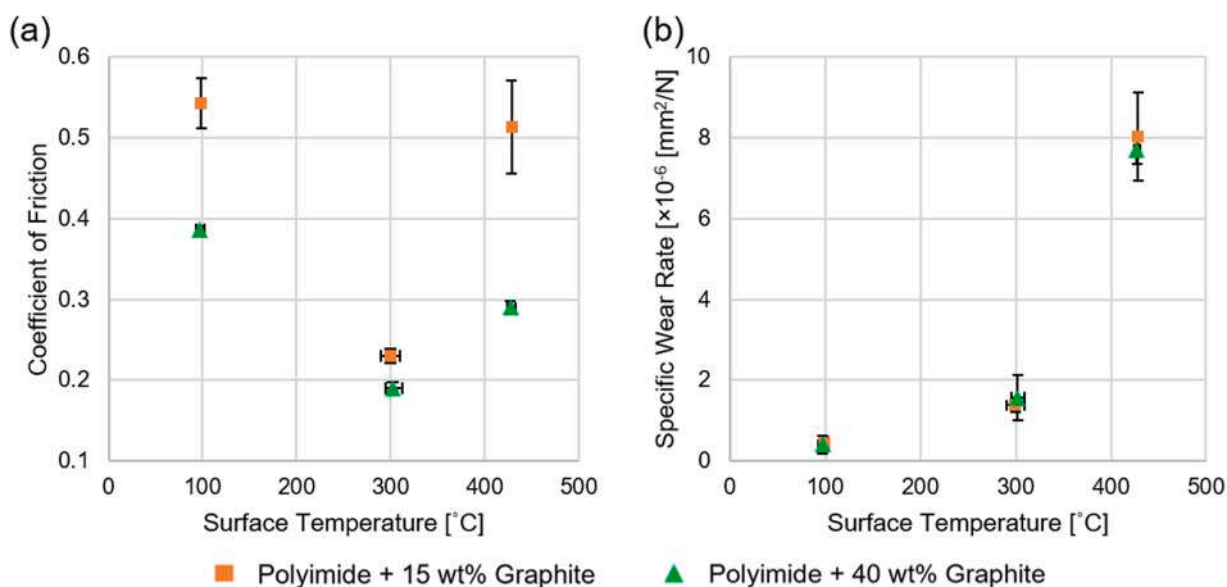
3.2.1. Misalignment of disc

Fig. 11 shows the SMAs of the coefficient of friction for graphite-filled PI/AISI 52100 sliding. Note that the 32 Hz vertical friction fluctuation, which has around 16 waves per rotation, is associated with the signal noise of the tribometer and should be ignored. In general, the SMAs show a 2 Hz vertical friction fluctuation, which has one wave per rotation. Low friction is observed from a position of 100° to 280° on the SMAs, whilst high friction is observed from 280° to 100°. This fluctuation is more significant as temperature increases. Since these friction variations manifest as vertical features on the SMAs, it suggests that events occur on the disc (refer to Fig. S1 in Supplementary Data). Fig. 12 (a) and (b) show the micrographs of the worn disc for 15 wt% graphite-filled PI/AISI 52100 sliding at 430 °C. Fig. 12(a) was taken at 80° on the wear track whilst Fig. 12(b) was taken at 215°. These correspond to the positions where elevated and reduced friction are found on the SMA (Fig. 12(c)) respectively. Before sliding, the AISI 52100 disc oxidises heavily at 430 °C and the surface is covered with a thick brown oxide layer. After sliding, it is found that the position with elevated friction has much less oxide on the disc surface compared to the position with reduced friction, which suggests that the elevated friction is due to oxide removal during sliding. The green sinusoidal line in Fig. 12(c) represents the measured average vertical pin position against the position on the disc. The fact that the pin position manifests as a single-cycle sinusoidal wave shows that the disc is misaligned, with the highest point found at 100° and the lowest point found at 280°. Elevated friction observed from 280° to 100° corresponds to the moment when the pin is going up the slope, whilst reduced friction observed from 100–280° corresponds to the moment when the pin is going down the slope. Friction is higher when the pin is going up the slope as more resistance is experienced by the pin due to the applied load and the 'cutting' angle, θ, as illustrated in Fig. 12(d) and (e).

Fig. 12(f) shows the graph of the difference in vertical pin position against temperature for graphite-filled PI/AISI 52100 sliding. The difference in pin position is the height difference between the highest and the lowest point on the disc, which represents how much the disc is misaligned. The misalignment increases as temperature increases, which explains why the friction variation becomes more obvious at higher temperatures. The increase in misalignment may be due to the bending of the spindle that drives the disc due to the differential thermal expansion, which is caused by uneven heating. A slight misalignment of

Fig. 10. Graphs of (a) coefficient of friction and (b) average specific wear rate for graphite-filled PI/AISI 52100 sliding against surface temperature. The standard deviation is plotted as the error bars in the graphs.

the disc is usually not a problem for a ball-on-disc sliding test at room temperature. However, when it comes to flat-on-flat sliding, high parallelism between the pin and the disc surfaces is required as even slight misalignment can lead to pressure concentration at the edge of the pin, leading to undesired local changes in tribological behaviours on the pin and/or the disc. This is even more so when the test is to be conducted at elevated temperatures, which could potentially amplify the misalignment. Without the SMA, such local events will often be overlooked and may eventually lead to the misinterpretation of the overall tribological phenomena.

3.2.2. Back-transfer film formation

The top-left image in Fig. 11, showing the friction SMA for PI with 15 wt% graphite at 100 °C, shows alternating horizontal intervals of reduced and elevated friction. The observed reduction of friction is approximately 15 – 20%. In Fig. 13(a), this SMA is shown next to the vertical pin position SMA (Fig. 13(b)). It can be seen that reduced friction corresponds to the pin being raised approximately 0.3 μm. It is hypothesised that these horizontal features indicate that substances adhere to the pin surface (refer to Fig. S2 in Supplementary Data). Fig. 13(c) shows the micrograph and (d) shows the height profile of the worn pin surface measured post-test. A film is observed on the pin surface (Fig. 13(c)) and the thickness of the film is approximately 0.3 μm

according to the bimodal height distribution (Fig. 13(d)). This film thickness agrees with how much the pin position is raised on the SMA. An EDS analysis of the surface indicates that the film is mainly made of carbon, nitrogen, and oxygen, whilst no significant iron is found. This indicates that the film is composed of PI which was once detached from the pin and has reattached, as schematically illustrated in Fig. 13(e). Similar film is also found in other polymers, e.g., PTFE [61], and such film is known as a back-transfer film, a secondary transfer film, or a running film. In an interrupted sliding test, it was shown that significant back-transfer films develop on the pin surface when friction is low, whilst no significant back-transfer film is found when friction is high (refer to Fig. S6 in Supplementary Data). This further confirms the lubricating effect of the back-transfer films. The alternating horizontal intervals of reduced and elevated friction found on the SMA suggests that the back-transfer film is constantly formed and removed during sliding, indicating its poor adhesion to the pin surface. The fact that the back-transfer film is only found for 15 wt% graphite at 100 °C suggests that low filler content and low temperature play a role in its formation.

3.3. Practical considerations in SMA analysis

Fig. 14 summarises several discussed manifestations in the SMA and their interpretation. These figures illustrate that spatiotemporal
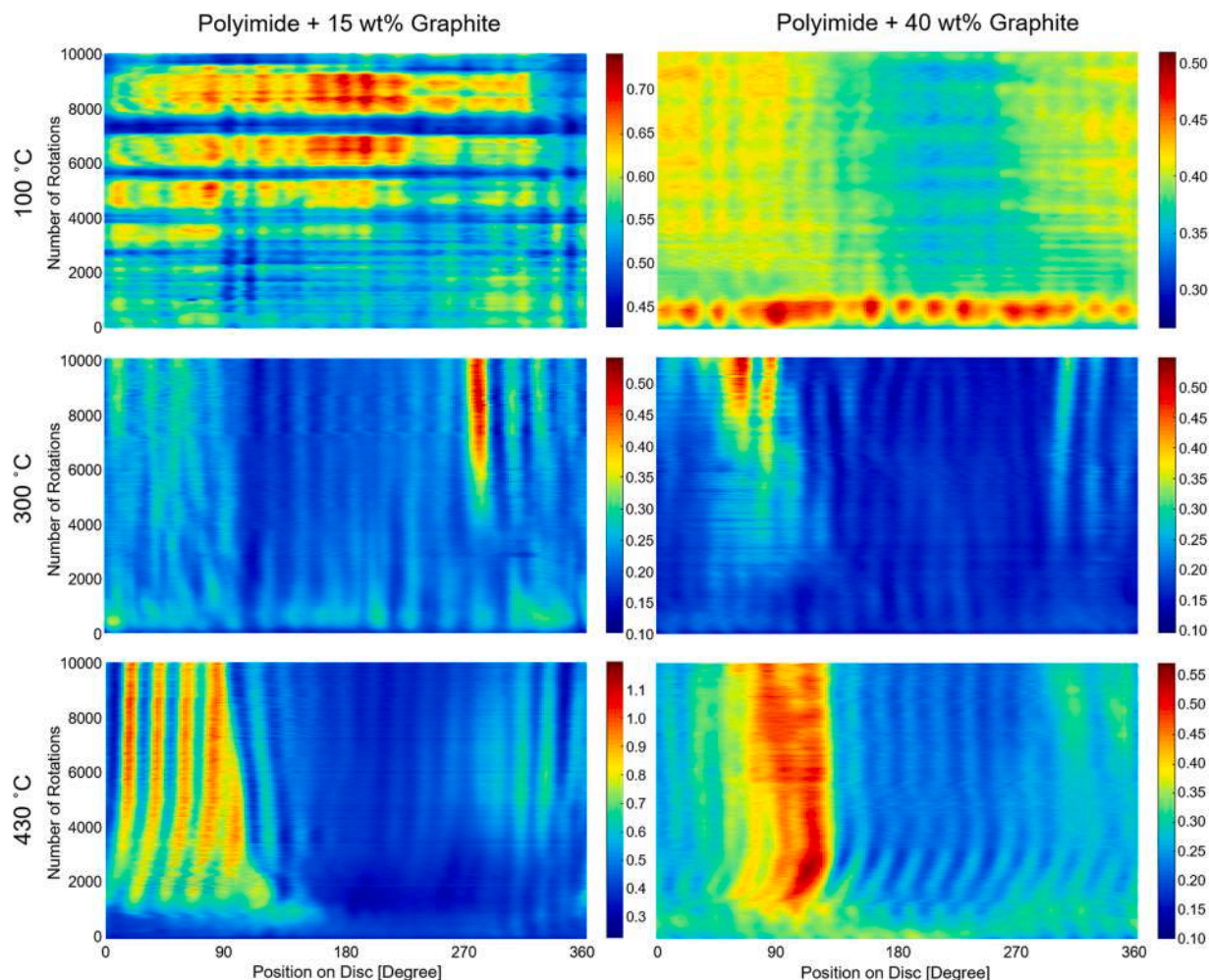
Fig. 11. SMAs of the coefficient of friction for graphite-filled PI/AISI 52100 sliding. Note that the 32 Hz vertical friction fluctuation, which has around 16 waves per rotation, is associated with the signal noise of the tribometer and should be ignored.
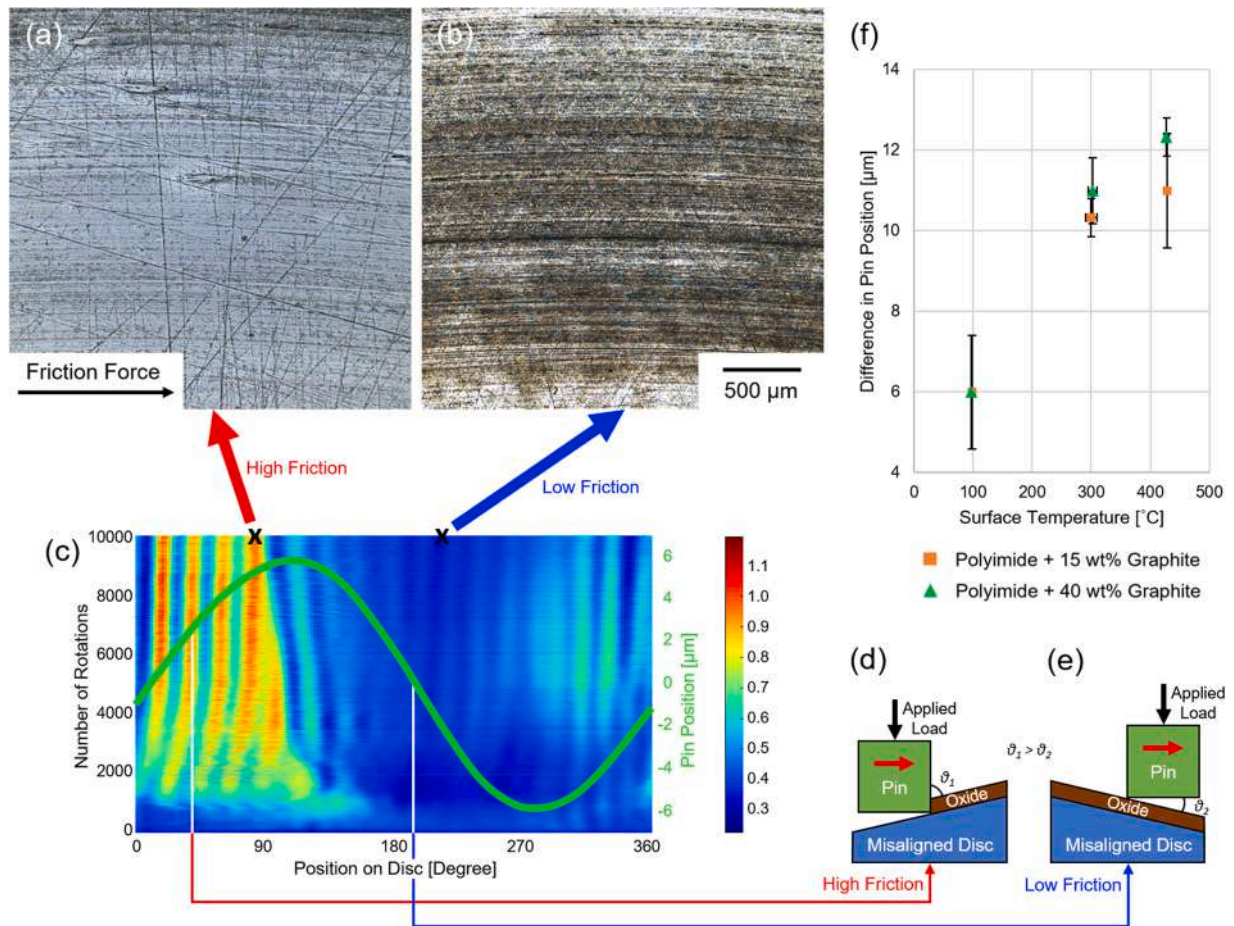
Fig. 12. Micrographs of the worn disc surface for 15 wt% graphite-filled PI/AISI 52100 sliding at 430 °C that were taken at (a) 80° and (b) 215° on the disc which corresponding to positions where high and low friction are found on (c) the SMA of the coefficient of friction respectively. The green sinusoidal line on the SMA represents the measured average vertical pin position against the position on the disc. (d) and (e) illustrate the cases when the oxide layer is removed when the pin is going up the slope of a misaligned disc but not removed when the pin is going down the slope. θ_1 and θ_2 represent the 'cutting' angle. (f) is the graph of the difference in vertical pin position against surface temperature for graphite-filled PI/AISI 52100 sliding. The standard deviation is plotted as the error bars in the graphs.
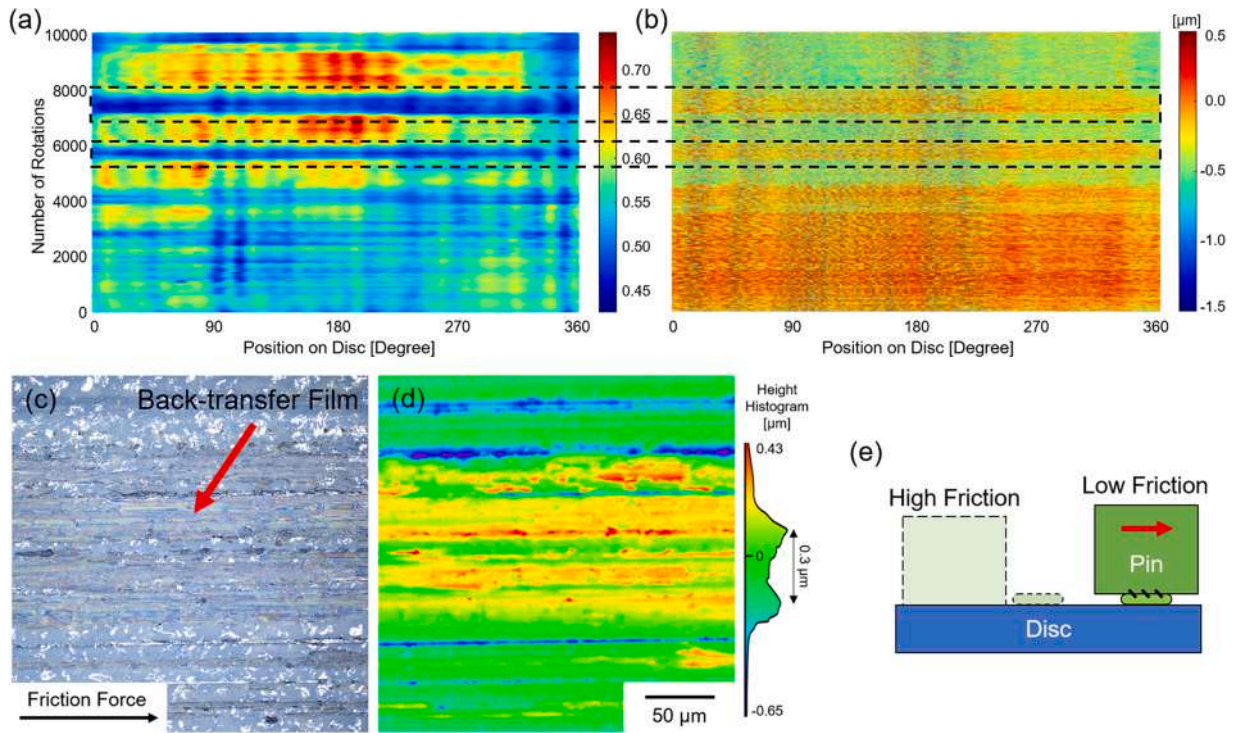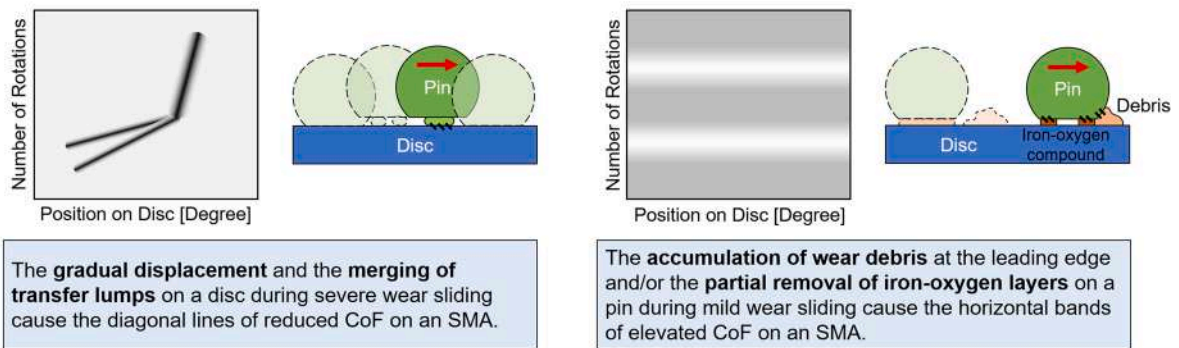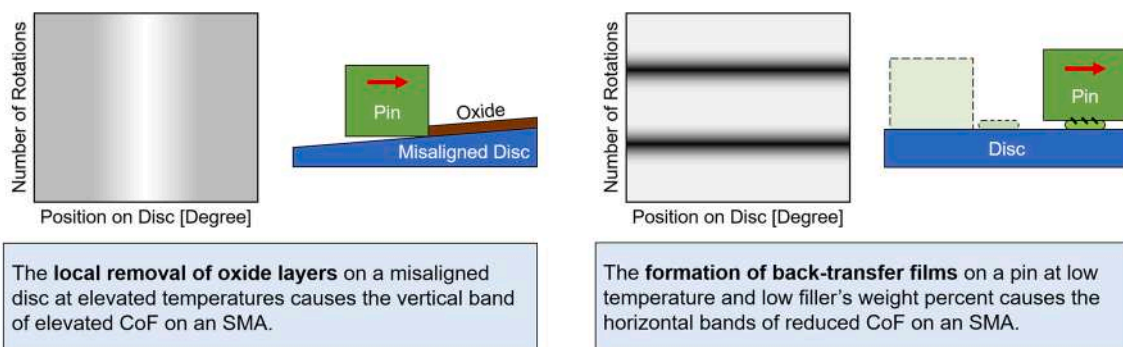
Fig. 13. SMAs of the (a) coefficient of friction and (b) vertical pin position and (c) micrograph and (d) height profile of the worn PI pin for 15 wt% graphite-filled PI/AISI 52100 sliding at 100 °C. The bimodal height histogram suggests the presence of a 0.3 μm thick film on the pin surface. (e) illustrates the case when a back-transfer film forms on the pin causing the friction to reduce. Note that the SMA of the pin position is filtered to remove the effect introduced by the misalignment of the disc.

1. Neat PTFE/AISI 304 Sliding

The **gradual displacement** and the **merging of transfer lumps** on a disc during severe wear sliding cause the diagonal lines of reduced CoF on an SMA.

The **accumulation of wear debris** at the leading edge and/or the **partial removal of iron-oxygen layers** on a pin during mild wear sliding cause the horizontal bands of elevated CoF on an SMA.

2. Graphite-filled Polyimide (PI)/AISI 52100 Sliding

The **local removal of oxide layers** on a misaligned disc at elevated temperatures causes the vertical band of elevated CoF on an SMA.

The **formation of back-transfer films** on a pin at low temperature and low filler's weight percent causes the horizontal bands of reduced CoF on an SMA.

* Colour bar for the spatiotemporal map (SMA) of the coefficient of friction (CoF): Low ▬▭ High

Fig. 14. Schematic overview of several SMA manifestations and their interpretations.

(a) How *T* can be can be related to *w*
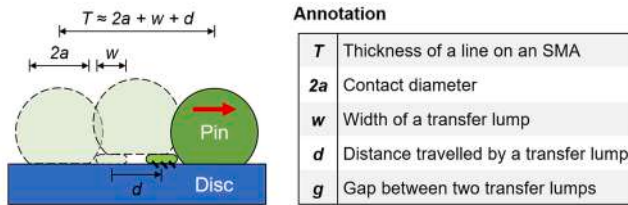
(b) How a phenomenon can be misinterpreted when *g < 2a*
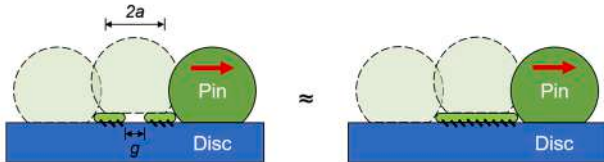
Fig. 15. Illustration of (a) how the thickness of a line on an SMA, T can be related to the width of a transfer lump, w and (b) how two closely separated transfer lumps can be misinterpreted as one larger lump on an SMA when the gap between two transfer lumps, g is smaller than the contact diameter, 2a.

mapping can provide detailed information on the dynamics of transfer substances in polymer/metal sliding, which would be overlooked when using conventional tribometry techniques. However, it is important to understand the specifications and limitations of the SMA analysis. An important aspect to consider is the spatial resolution, which is the smallest feature that can be resolved accurately by the sensors on a tribometer and which depends on the sampling interval and the contact diameter.

The sampling interval of an SMA is the distance between two acquired samples on the disc. It needs to be at least smaller than the feature of interest in order for the sensors to pick up its signals and to manifest on an SMA. The contact diameter between the pin and the disc decides how accurate and how distinct or sharp the manifested feature is on the SMA. If a transfer lump with a width w is moved over a distance d by the pin with a contact diameter of $2a$, a line with a thickness of $T \approx 2a + w + d$ will be displayed on the SMA as shown in Fig. 15(a). This means that a manifested feature on the SMA will appear blurred and larger than it actually is. Since the distance travelled by a transfer lump, d is a variable that depends on the tribological conditions in the contact, the only way to minimise 'blurriness' (or the deviation between T and w) is by reducing the contact diameter, $2a$. A large contact diameter will not only cause blurriness but could also mask important features on the disc, leading to misinterpretation of results, for instance by incorrectly interpreting two lumps on the surface as one, which would occur if the gap between the two lumps, g is smaller than $2a$ (Fig. 15(b)). In a typical ball-on-flat contact, the contact diameter increases with time as wear progresses. This means that the spatial resolution will deteriorate with time during a sliding test. Any quantitative analysis on an SMA should be performed with these considerations in mind.

4. Conclusions

Spatiotemporal mapping provides insight to tribological events happening locally in the space and time domains. Together with post-hoc surface characterisation techniques, spatiotemporal mapping can be a powerful tool to better understand the transfer mechanisms in polymer/metal contacts. Two tribological systems were explored in this study. In a PTFE/stainless steel system, spatiotemporal mapping helps clarify how the competition between the transfer of PTFE to the disc and the transfer of iron to the pin governs the severe-to-mild wear transition of PTFE and how the amount of existing oxide on the disc and humidity can promote the transition. It also helps establish a hypothesis for the

slide-roll mechanism of PTFE transfer lumps on the disc during severe wear. In a PI/bearing steel system, spatiotemporal mapping helps spot the formation of back-transfer films on the pin which could potentially reduce friction significantly. Additionally, spatiotemporal mapping is found useful in detecting abnormal tribological behaviour, such as the local removal of the oxide layer due to the misalignment of the disc at elevated temperatures. Many of these phenomena would otherwise be overlooked without spatiotemporal mapping.

CRediT authorship contribution statement

Kian Kun Yap: Conceptualization, Software, Validation, Formal analysis, Investigation, Data curation, Writing – original draft, Writing – review & editing, Visualization, Project administration. **Kanao Fukuda:** Methodology, Software, Writing – review & editing, Supervision. **Jennifer Renee Vail:** Resources, Writing – review & editing. **Janet Wong:** Writing – review & editing, Supervision. **Marc Arthur Masen:** Conceptualization, Writing – review & editing, Supervision, Funding acquisition.

Declaration of Competing Interest

The authors declare that they have no known competing financial interests or personal relationships that could have appeared to influence the work reported in this paper.

Appendix A. Supporting information

Supplementary data associated with this article can be found in the online version at doi:10.1016/j.triboint.2022.107533.

References

[1] Friedrich K. Friction and Wear of Polymer Composites. Amsterdam: Elsevier; 1986. https://doi.org/10.1016/0266-3538(87)90078-9.
[2] Batchelor AW, Stachowiak GW. Wear of Non-metallic Materials. Eng. Tribol. Oxford: Elsevier; 2014. p. 679. https://doi.org/10.1016/B978-0-12-397047-3.00016-3.
[3] Bowden FP, Tabor D. Mechanism of metallic friction. Nature 1942;150:197–9. https://doi.org/10.1038/150197a0.
[4] Bowden FP, Tabor D. The Friction and Lubrication of Solids. Clarendon Press; 1986.
[5] Pooley CM, Tabor D. Friction and molecular structure: The behaviour of some thermoplastics. Proc R Soc Lond A Math Phys Sci 1972;329:251–74. https://doi.org/10.1098/rspa.1972.0112.
[6] Briscoe B. Wear of polymers: an essay on fundamental aspects. Tribol Int 1981;14: 231–43. https://doi.org/10.1016/0301-679X(81)90050-5.
[7] Tanaka K. Transfer of semi-crystalline polymers sliding against smooth steel surface. Wear 1982;75:183–99. https://doi.org/10.1016/0043-1648(82)90147-8.
[8] Jean-Fulcrand A, Masen MA, Bremner T, Wong JSS. Effect of temperature on tribological performance of polyetheretherketone-polybenzimidazole blend. Tribol Int 2019;129:5–15. https://doi.org/10.1016/J.TRIBOINT.2018.08.001.
[9] Laux KA, Schwartz CJ. Effects of contact pressure, molecular weight, and supplier on the wear behavior and transfer film of polyetheretherketone (PEEK). Wear 2013;297:919–25. https://doi.org/10.1016/j.wear.2012.11.013.
[10] Laux KA, Schwartz CJ. Influence of linear reciprocating and multi-directional sliding on PEEK wear performance and transfer film formation. Wear 2013;301: 727–34. https://doi.org/10.1016/j.wear.2012.12.004.
[11] Yap KK. Tribology of aerospace materials. MSc Thesis. Imperial College London, 2019.
[12] Yap KK, Masen MA. Effect of temperature and filler on the tribological responses of sintered polyimides. Proc. STLE Tribol. Front. Virtual Conf., 2020.
[13] Jean-Fulcrand A, Masen MA, Bremner T, Wong JSS. High temperature tribological properties of polybenzimidazole (PBI). Polymer 2017;128:159–68. https://doi.org/10.1016/J.POLYMER.2017.09.026.
[14] Kim Y-J, Jung H, Han SW, Kwon O-H. Ultrafast electron microscopy visualizes acoustic vibrations of plasmonic nanorods at the interfaces. Matter 2019;1:481–95. https://doi.org/10.1016/j.matt.2019.03.004.

[15] Newacheck S, Youssef G. Noncontact spatiotemporal strain mapping of composite multiferroic cylinders. Int J Mech Mater Des 2020. https://doi.org/10.1007/s10999-020-09502-0.

[16] Dinning PG, Zarate N, Hunt LM, Fuentealba SE, Mohammed SD, Szczesniak MM, et al. Pancolonic spatiotemporal mapping reveals regional deficiencies in, and disorganization of colonic propagating pressure waves in severe constipation. Neurogastroenterol Motil 2010;22:e340–9. https://doi.org/10.1111/j.1365-2982.2010.01597.x.

[17] Roberts RR, Bornstein JC, Bergner AJ, Young HM. Disturbances of colonic motility in mouse models of Hirschsprung's disease. Am J Physiol Liver Physiol 2008;294: G996–1008. https://doi.org/10.1152/ajpgi.00558.2007.

[18] Le Lay H, Thomas Z, Rouault F, Pichelin P, Moatar F. Characterization of diffuse groundwater inflows into stream water (part II: quantifying groundwater inflows by coupling FO-DTS and vertical flow velocities). Water 2019;11:2430. https://doi.org/10.3390/w11122430.

[19] He Z, Lei L, Zhang Y, Sheng M, Wu C, Li L, et al. Spatio-temporal mapping of multi-satellite observed column atmospheric CO_2 using precision-weighted Kriging method. Remote Sens 2020;12:576. https://doi.org/10.3390/rs12030576.

[20] Kilibarda M, Hengl T, Heuvelink GBM, Gräler B, Pebesma E, Perčec Tadić M, et al. Spatio-temporal interpolation of daily temperatures for global land areas at 1 km resolution. J Geophys Res Atmos 2014;119:2294–313. https://doi.org/10.1002/2013JD020803.

[21] Chattopadhyay A, Hassanzadeh P, Pasha S. Predicting clustered weather patterns: a test case for applications of convolutional neural networks to spatio-temporal climate data. Sci Rep 2020;10:1317. https://doi.org/10.1038/s41598-020-57897-9.

[22] Belin M, Martin JM. Triboscopy, a new approach to surface degradations of thin films. Wear 1992;156:151–60. https://doi.org/10.1016/0043-1648(92)90150-7.

[23] Fukuda K. Friction force measurement methods and its measuring devices. Japanese Patent 208949, 1992.

[24] Dos Santos MB, Costa HL, De Mello JDB. Potentiality of triboscopy to monitor friction and wear. Wear 2015;332–333:1134–44. https://doi.org/10.1016/j.wear.2014.10.017.

[25] Fukuda K. Pin-on-disk tribo-tester with spatiotemporal mapping analysis. Mytribos Symp 2, Skudai 2017:51–3.

[26] K. Fukuda, T. Morita, J. Sugimura, Analysis of friction and wear in hydrogen environment using friction force and specimen displacement maps. Proc Jpn Soc Tribol Conf, Tokyo, 2008, pp. 21–22.

[27] Ali NM, Fukuda K, Chai CY, Yamazaki T. Spatiotemporal mapping analysis on the sliding behavior of steels with different hardness. Proc Asia Int Conf Tribol, Kuching 2018:480–1.

[28] Fukuda K, Morita T. Fundamental physical mechanisms of adhesive wear identified with spatiotemporal mapping analysis. Proc Asia Int Conf Tribol, Kuching 2018: 398–9.

[29] Fukuda K. Friction force distribution and its alternation with repeated sliding. Jpn J Tribol 1998;43:1143–55.

[30] N.M. Ali, K. Fukuda, T. Morita, Z.A. Subhi, Spatiotemporal mapping analysis on tribo-data in boundary lubrication. Proc 5th Malays-Jpn Tribol Symp, Kuala Lumpur, 2017, pp. 8-9.

[31] Fukuda K. Combinational analysis of multi-data obtained in a repeated sliding system. Wear 2008;264:499–504. https://doi.org/10.1016/j.wear.2007.04.002.

[32] Belin M, Lopez J, Martin JM. Triboscopy, a quantitative tool for the study of the wear of a coated material. Surf Coat Technol 1994;70:27–31. https://doi.org/10.1016/0257-8972(94)90070-1.

[33] Belin M. Triboscopy: A new quantitative tool for microtribology. Wear 1993;168: 7–12. https://doi.org/10.1016/0043-1648(93)90190-W.

[34] Fontaine J, Belin M, Le Mogne T, Grill A. How to restore superlow friction of DLC: The healing effect of hydrogen gas. Tribol Int 2004;37:869–77. https://doi.org/10.1016/j.triboint.2004.07.002.

[35] Sánchez-López JC, Belin M, Donnet C, Quirós C, Elizalde E. Friction mechanisms of amorphous carbon nitride films under variable environments: A triboscopic study. Surf Coat Technol 2002;160:138–44. https://doi.org/10.1016/S0257-8972(02)00397-3.

[36] Wahl KJ, Belin M, Singer IL. A triboscopic investigation of the wear and friction of MoS2 in a reciprocating sliding contact. Wear 1998;214:212–20. https://doi.org/10.1016/S0043-1648(97)00246-9.

[37] Loubet JL, Belin M, Durand R, Pascal H. Triboscopic description of local wear phenomena under an AFM tip. Thin Solid Films 1994;253:194–8. https://doi.org/10.1016/0040-6090(94)90319-0.

[38] De Oliveira MM, Costa HL, Silva WM, De Mello JDB. Effect of iron oxide debris on the reciprocating sliding wear of tool steels. Wear 2019;426–427:1065–75. https://doi.org/10.1016/j.wear.2018.12.047.

[39] Barbosa LM, Da Silva WM, De Mello JDB. Orthomicrotribometer. Wear 2019; 426–427:1729–39. https://doi.org/10.1016/j.wear.2018.12.067.

[40] Costa HL. Oliveira Junior MM, De Mello JDB. Effect of debris size on the reciprocating sliding wear of aluminium. Wear 2017;376–377:1399–410. https://doi.org/10.1016/j.wear.2016.10.025.

[41] Goncalves JL, De Mello JDB, Costa HL. Tribological behaviour of alternative surface modifications for cold rolling mill rolls. Wear 2021;470–471:203614. https://doi.org/10.1016/j.wear.2021.203614.

[42] Fukuda K, Subhi ZA, Morita T. Analytical study on the growth and transfer of adhesive substances generated on the surface in the early stage of sliding. Wear 2015;330–331:64–9. https://doi.org/10.1016/j.wear.2014.11.009.

[43] A Manaf ND, Fukuda K, Subhi ZA, Mohd Radzi MF. Influences of surface roughness on the water adsorption on austenitic stainless steel. Tribol Int 2019;136:75–81. https://doi.org/10.1016/j.triboint.2019.03.014.

[44] DuPont Inc. Teflon PTFE fluoropolymer resin properties handbook. 2020.

[45] Ye J, Sun W, Zhang Y, Liu X, Liu K. Measuring evolution of transfer film–substrate interfaceusing low wear alumina PTFE. Tribol Lett 2018;66:1–14. https://doi.org/10.1007/s11249-018-1054-6.

[46] Stachowiak GW, Batchelor AW, Stachowiak GB. Control of the test environment. Experimental Methods in Tribology. Amsterdam: Elsevier; 2004. p. 103–14.

[47] Meylan B, Ciani D, Zhang B, Cuche E, Wasmer K. A new ball-on-disk vacuum tribometer with in situ measurement of the wear track by digital holographic microscopy. Surf Topogr Metrol Prop 2017;5:044004. https://doi.org/10.1088/2051-672x/aa854a.

[48] Hutchings I. Tribology: Friction and Wear of Engineering Materials. London: Edward Arnold; 1992.

[49] Campbell KL, Sidebottom MA, Atkinson CC, Babuska TF, Kolanovic CA, Boulden BJ, et al. Ultralow wear PTFE-based polymer composites - the role of water and tribochemistry. Macromolecules 2019;52:5268–77. https://doi.org/10.1021/acs.macromol.9b00316.

[50] Wang H, Li H, Yan F. Reduction in wear of metakaolinite-based geopolymer composite through filling of PTFE. Wear 2005;258:1562–6. https://doi.org/10.1016/j.wear.2004.11.001.

[51] Ye J, Tao B, Sun W, Haidar DR, Alam KI, Liu K, et al. The competing effects of counterface peaks and valleys on the wear and transfer of ultra-low wear alumina–PTFE. Tribol Lett 2018;66:1–14. https://doi.org/10.1007/s11249-017-0966-x.

[52] Ye J, Wei J, Zeng J, Alam KI, Sun W, Liu X, et al. Interfacial gradient and its role in ultralow wear sliding. ACS Appl Mater Interfaces 2020. https://doi.org/10.1021/acs.jpcc.9b12036.

[53] Khare HS, Moore AC, Haidar DR, Gong L, Ye J, Rabolt JF, et al. Interrelated effects of temperature and environment on wear and tribochemistry of an ultralow wear PTFE composite. J Phys Chem C 2015;119:16518–27. https://doi.org/10.1021/acs.jpcc.5b00947.

[54] DuPont Inc. Vespel S line design handbook. 2019.

[55] Lancaster JK. Abrasive wear of polymers. Wear 1969;14:223–39. https://doi.org/10.1016/0301-679X(82)90054-8.

[56] Tewari US, Bijwe J. On the abrasive wear of some polyimides and their composites. Tribol Int 1991;24:247–54. https://doi.org/10.1016/0301-679X(91)90051-A.

[57] Samyn P, Schoukens G. Tribochemical reactions on polyimide sliding surfaces evaluated with Raman spectroscopy and atomic force microscopy. Surf Interface Anal 2008;40:853–7. https://doi.org/10.1002/sia.2706.

[58] Samyn P, Schoukens G, Verpoort F, Van Craenenbroeck J, De Baets P. Friction and wear mechanisms of sintered and thermoplastic polyimides under adhesive sliding. Macromol Mater Eng 2007;292:523–56. https://doi.org/10.1002/mame.200600400.

[59] Samyn P, Schoukens G, Quintelier J. Tribophysical interpretation of polymer sliding mechanisms. Polym. Tribol. London: Imperial College Press,; 2009. p. 38–73.

[60] Samyn P, Vancraenenbroeck J, Verpoort F, De Baets P. Postmortem Raman spectroscopy explaining friction and wear behavior of sintered polyimide at high temperature. J Mater Eng Perform 2006;15:750–7. https://doi.org/10.1361/105994906×150885.

[61] Ye J, Burris DL, Xie T. A review of transfer films and their role in ultra-low-wear sliding of polymers. Lubricants 2016;4:1–15. https://doi.org/10.3390/lubricants4010004.